High Temperature Oxidation Behavior of Fe- and Ni-Based Alloy Foils in Water Vapor at 850 °C

Marie Romedenne
Materials Science and Technology Division,
Oak Ridge National Laboratory, Oak Ridge, TN
37831-6156, United States

Sebastien Dryepondt
Materials Science and Technology Division,
Oak Ridge National Laboratory, Oak Ridge, TN
37831-6156, United States

Rishi Pillai
Materials Science and Technology Division,
Oak Ridge National Laboratory, Oak Ridge, TN
37831-6156, United States

Michael Lance
Materials Science and Technology Division,
Oak Ridge National Laboratory, Oak Ridge, TN
37831-6156, United States

Bruce Pint
Materials Science and Technology Division,
Oak Ridge National Laboratory, Oak Ridge, TN
37831-6156, United States

ABSTRACT

Operating temperatures above 700°C are desired to improve the efficiency of power generation systems such as microturbines. Therefore, the use of creep-resistant Ni-based or Fe-based alloys, which can form protective Cr_2O_3 and Al_2O_3 scales, is required. In this paper, Fe- and Ni-based alloy foils were oxidized in air + 10 % H_2O for up to 3,000 h at 850°C to identify the most promising alloys. The thickness and chemical composition of the spinel oxide formed on top of the Cr_2O_3 scale varied between S3100, N08120 and N06230 alloy foils. In addition, the rate of Cr and Mn loss (spinel and Cr_2O_3 oxidation and volatilization) or Al loss (oxidation) and the dissolution of strengthening precipitates, were found to be a function of the nature of the formed oxide (Fe or Ni-rich spinel, Cr_2O_3, Al_2O_3). Alloys N06230 and alumina-forming austenitic (AFA) steels were found to be well-suited for the applications as microturbine recuperator foil materials up to 850˚C.

Keywords: Foil, Oxidation, Water vapor, Metal loss

INTRODUCTION

Decreased cost and enhanced electrical efficiency (currently < 35 %) of recuperated microturbines are essential for their widespread use as power generation systems [1, 2]. To further increase efficiency, research has been conducted towards increasing the microturbine's turbine inlet

temperature such that the outlet temperature to the recuperator would be above 750˚C [1] (currently ~650°C) and optimizing the design of compact microturbine recuperators [3]. Recuperator temperatures over 600˚C have been shown to challenge the oxidation lifetime of S34700 stainless steel foils used in primary surface recuperators [4-6]. Therefore, microturbine manufacturers have used Ni-based alloys such as N08120 and N06625 and advanced austenitics (S31025) to achieve ~650°C operation [7]. A key issue is that microturbine exhaust gas contains water vapor which could decrease the oxidation lifetime of Cr_2O_3-forming alloys such as S30400 or N06625 due to the formation of volatile $CrO_2(OH)_2$ [8, 9].

Greater Cr depletion was reported for the S30403 steel coupon after 679 h of exposure in flowing O_2 + 10 % H_2O (100 $mL.min^{-1}$ / 2.5 $cm.s^{-1}$) at 600°C in comparison to dry air [8]. The cyclic oxidation behaviors of austenitic and ferritic Fe-(10-30)Ni-(10-20)Cr model alloys were studied between 650 and 800˚C in air + 10 % H_2O (1h cycle) [10]. The presence of higher Ni and Cr contents was reported to delay the transition time from protective oxidation behavior, characterized by Cr_2O_3 formation, to accelerated attack with the formation of Fe and Cr-rich oxides [10]. The effect of water vapor on the oxidation behavior on commercial Ni-based materials was studied by several authors [11-14]. The extent of Cr depletion in N06625 coupon exposed for 1,000 h in flowing air + 6 % H_2O at 900 ˚C was reported to increase with increasing gas flow rate from 0.5 to 600 $cm.s^{-1}$ [11]. The presence of water vapor led to the formation of large Fe-rich nodules on the surface of Fe-25Ni-20Cr foils oxidized in air + 10 % H_2O at 650, 700 and 800˚C and increased Cr depletion within the foils [12,13]. The oxidation resistance of Cr_2O_3 and Al_2O_3 forming foils was compared after exposure in flowing air + 10 % H_2O (500 $cm^3.min^{-1}$) studied between 760 and 871˚C up to 8,640 h (360 days) [14]. At 760˚C, the S34700 stainless steel foil underwent breakaway oxidation after about 720 h. The N08120, N06002, N06625 and N06230 specimens presented similar mass change (less than 0.5 $mg.cm^{-2}$ after 8,640 h) and comparable oxidation attack parameter (defined by the authors as the product of original foil thickness and average metal depth affected by oxidation and internal oxidation) were observed between for N08120, N06002 and N06625 alloys [14]. After 8,640 h exposure at 871˚C, attack parameters were the highest for 347 stainless steel, alloy N08120 and alloy N07208, the lowest being for the alloys N06230, N06625 and N06002 [14]. In the study, the alumina forming alloy N07214 exhibited the lowest oxidation attack parameters at all temperatures due to the formation of an external Al_2O_3 scale [14].

Since the volatilization of the Cr_2O_3 scale was shown to decrease the lifetime of some Cr_2O_3 forming alloys, extensive research has been conducted towards the development of creep resistant alumina forming austenitic (AFA) steels which are also less expensive than Ni-based alloys [15,16]. Previous studies included laboratory exposures at 650° - 800°C where commercial AFA foils, 80-150 µm thick, demonstrated protective oxidation behaviors up to 10,000 h at 800˚C [17,18] and longer exposures in engine tests [18].

The objective of this study was to identify potential oxidation and creep resistant materials to be employed as microturbine recuperator foils at even higher temperatures (T > 800°C). Therefore, the oxidation and volatilization behaviors of several Fe and Ni-based chromia forming foils and Fe-based alumina forming foils were compared in flowing air + 10 % H_2O at 850 ˚C. The oxidation induced Cr or Al depletion, sound metal loss, and dissolution of strengthening precipitates were characterized.

EXPERIMENTAL PROCEDURE

Materials

Several chromia-forming alloy foils (compositions shown in Table 1) were oxidized in dry air in a resistively heated box furnace up to 7,000 h at 800 ˚C and up to 500 h at 850˚C using 100-h cycles. The specimens were also exposed in a resistively heated alumina tube furnace (diameter of 5.9 cm) with flowing (850 $cm^3.min^{-1}$, velocity of 1.95 $cm.s^{-1}$) air + 10 % H_2O (g) (referred to as wet air) in
100 h-cycles up to 7,000 h at 800˚C and up to 3,000 h at 850°C. A detailed description of the experimental procedure is available in [12]. The Fe-based and Ni-based foils presented a bright surface finish and were cut into ~20mmx10mm size (thickness shown in
Table 3), and then ultrasonically cleaned in acetone and ethanol prior to oxidation exposure.

Table 1: Composition of Fe and Ni based alloys (in wt.%) analyzed by inductively coupled plasma–optical emission spectrometry (ICP–OES) and combustion analysis.

Alloy/ wt.%	Ni	Cr	Fe	Mo	Nb	Co	Mn	Si	W	Al	Ti	La	C
	Fe-based alloy												
S31000	19.5	24.1	54.0	0.07	0.01	0.05	1.66	0.33	-	0.01	0.01	-	0.05
	Ni-based alloys												
N08120	39.5	25.8	32.2	0.45	0.42	0.09	0.52	0.33	0.1	0.04	0.01	-	0.05
N06230	58.2	22.3	1.03	1.17	0.02	1.07	0.67	0.42	14.5	0.37	0.01	0.02-0.05	0.09
N06625	61.6	21.4	4.31	8.39	3.43	0.09	0.08	0.09	0.01	0.11	0.19	-	0.06

Fe-based commercial AFA (AFA1) and laboratory made AFA (AFA2) were also investigated (compositions in Table 2). Native oxides were present on the surface of the AFAs which were homogenized (2h), hot-forged, hot-rolled, cold-rolled and annealed for 1h at 1100 ˚C and cut into 20mmx10mm foils (thicknesses shown in
Table 3).

Table 2: Composition of Fe based alumina former alloys (in wt.%) analyzed by inductively coupled plasma–optical emission spectrometry (ICP–OES) and combustion analysis.

Fe based alloys												
Alloy/ wt.%	**Ni**	**Cr**	**Fe**	**Mo**	**Nb**	**Co**	**Mn**	**Si**	**W**	**Al**	**Ti**	**C Zr Y Hf**
AFA1	25.1	14.9	base	2.01	2.50		1.93	0.15	-	3.98	-	0.09 - 0.009 0.14
AFA2	25.0	14.0	49.66	1.99	2.53	-	2.0	0.16	0.97	3.57	0.05	0.10 - - -

Table 3: Thickness of the studied foils

Alloy	Foil thickness (µm)
S31000	51 ± 5
N08120	85 ± 15
N06230	200 ± 10

N06625	100 ± 20
AFA1 (commercial)	80 ± 5
AFA2 (laboratory made)	120 ± 10

Characterizations

After the oxidation exposure, specimens were Cu plated and mounted in conductive epoxy for cross sectional characterization including Scanning Electron, Back-scattered Electron Microscopy (BSE) (TESCAN MIRA3 SEM), energy dispersive X-ray spectroscopy (EDAX Octane Elect Super Silicon Drift Detector) and electron probe microanalysis (EPMA JEOL 8200/8500).

RESULTS

Mass change

Short-term oxidation

The mass change of the studied materials after exposure in dry air at 850˚C is reported in Figure 1a. No spallation of the oxide scale formed on the specimens was observed in dry and wet air exposures. The S31000 specimen exhibited higher mass gains than the N08120, N06625 and N06230. The alloys N06625 and N06230 showed the lowest mass gain up to 500 h.

No significant differences in the mass change were observed for the S31000, N06230 and N08120 specimens in wet air compared to the dry air exposure (Figure 1b). For the N06625 foil, a mass loss of -0.1 mg.cm^{-2} was measured in wet air after 500 h (Figure 1b), but a mass gain of 0.1 mg.cm^{-2} was observed in dry air (Figure 1a). The AFA foil specimens were not tested in dry air and exhibited low mass change in wet air (Figure 1b).

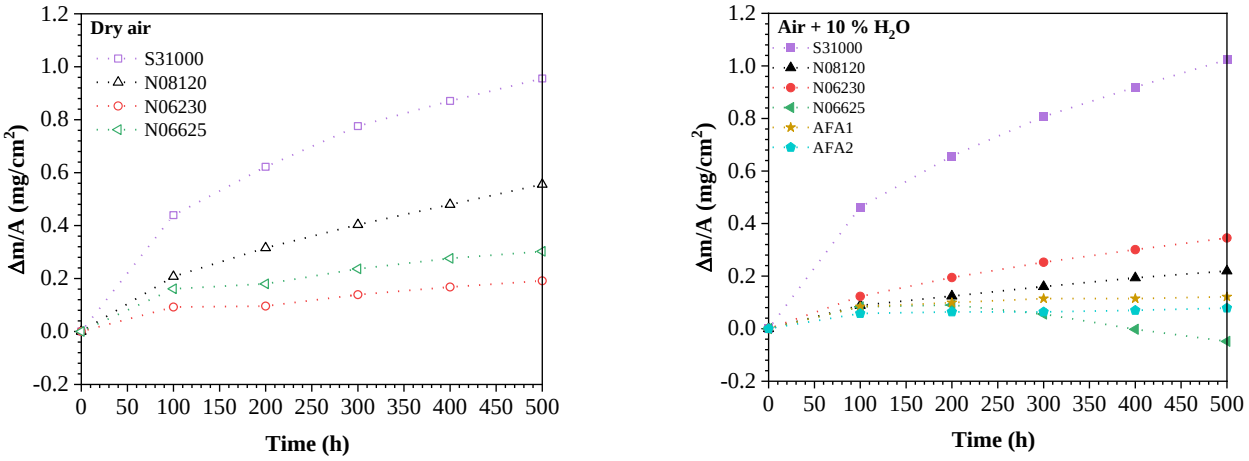

(a) (b)

Figure 1: Specimens mass change after 100 h cyclic exposure in (a) dry air and (b) in flowing air + 10% H_2O at 850˚C.

Long-term oxidation behavior

Similar trends in the mass change behavior were observed between the short-term and long-term oxidation tests. The S31000 foil continued to exhibit a large mass gain to reach about 5 mg.cm^{-2} after 3,000 h (Figure 2). For the N08120, N06230, AFA1 and AFA2 mass gains were observed up to

3,000 h. The lowest mass gains were 0.2 mg.cm^{-2} after 3,200 h for the AFA1 specimens and 0.1 mg.cm^{-2} after 3,000 h for the AFA2 specimens. For the alloy N06625, after an initial mass gain for 300-400 h, a linear mass loss was measured.

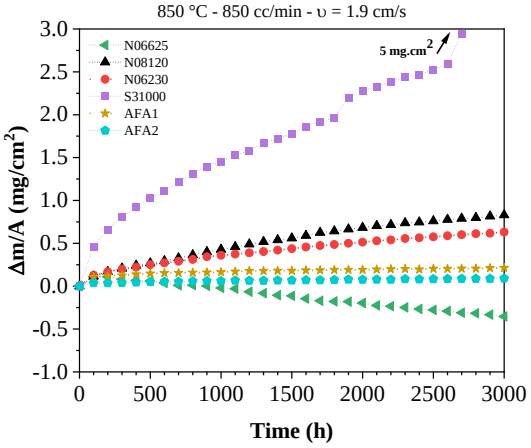

Figure 2: Mass change of specimens after 3,000 h after 100 h cycle exposure in air + 10 % H_2O at 850˚C.

Oxide scale characterization

BSE images of the cross-sections of the specimens after 1,000 h exposures in wet air at 850 ˚C are reported in Figure 3. For the S31000, N08120 and N06230 specimens, spinel oxides formed on top of a Cr-rich scale (likely Cr_2O_3). The thickness of the oxide scale formed on the S31000 specimen was greater (9 ± 1 µm) than that on the alloys N08120 (4 ± 1 µm) and N06230 (2.5 ± 0.5 µm). The spinel-type oxide scale formed on the surface of the Cr_2O_3 scale of S31000 and N08120 specimens were Mn, Cr and Fe-rich (Figure 4a,b). On the N06230 foil, a Mn, Cr, Fe and Ni-rich spinel was found (Figure 4c).

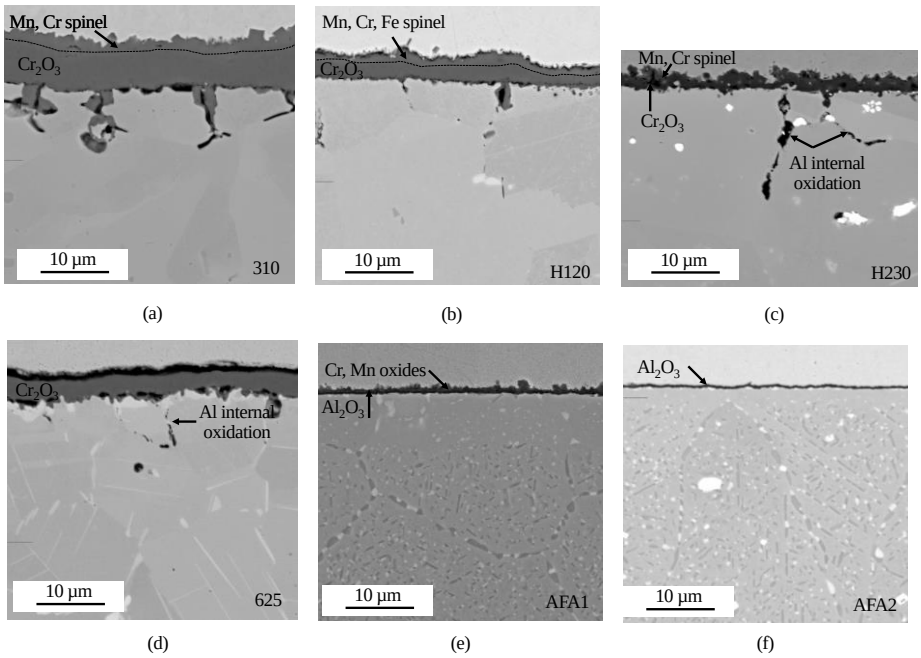

Figure 3: BSE images of (a) S31000, (b) N08120, (c) N06230, (d) N06625, (e) AFA1 and (f) AFA2 after 1,000 h of exposure in 100 h cycle flowing air + 10 % H_2O at 850˚C.

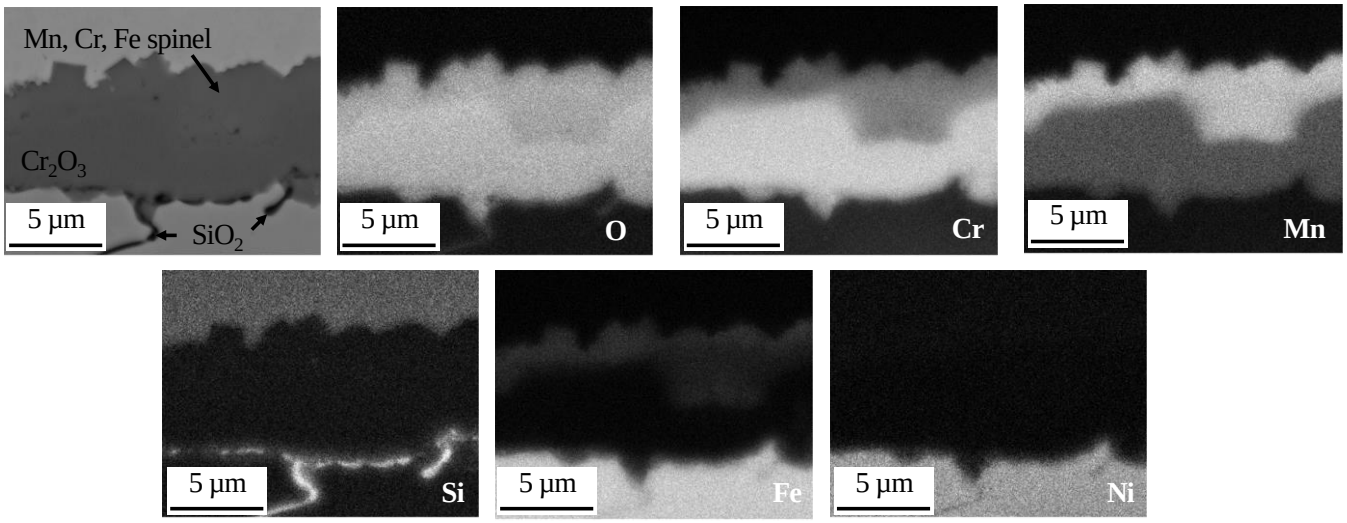

(a)

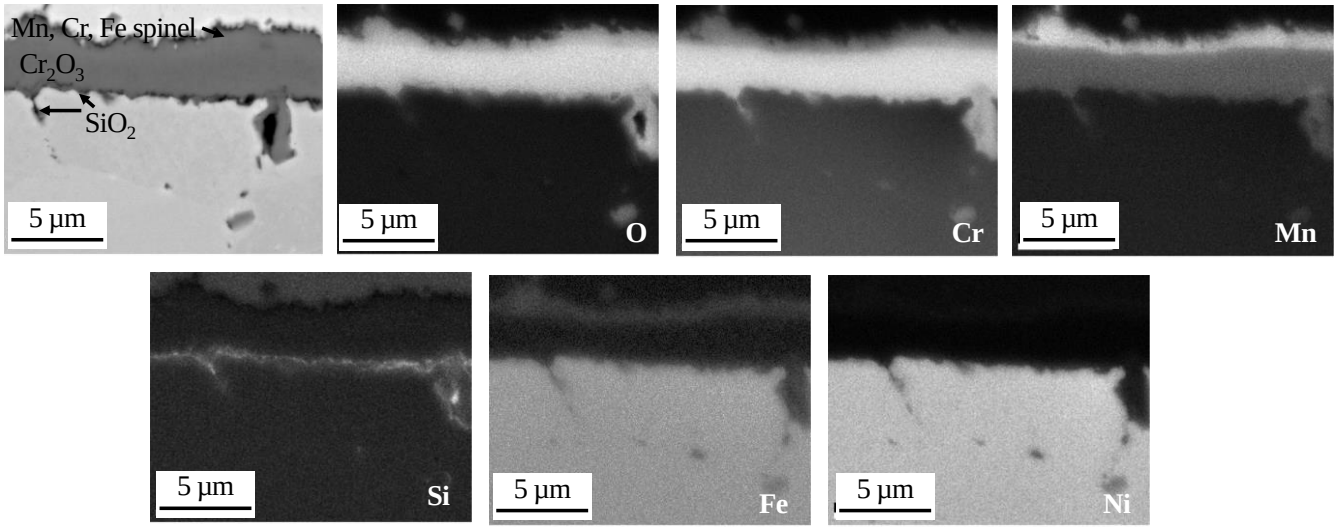

(b)

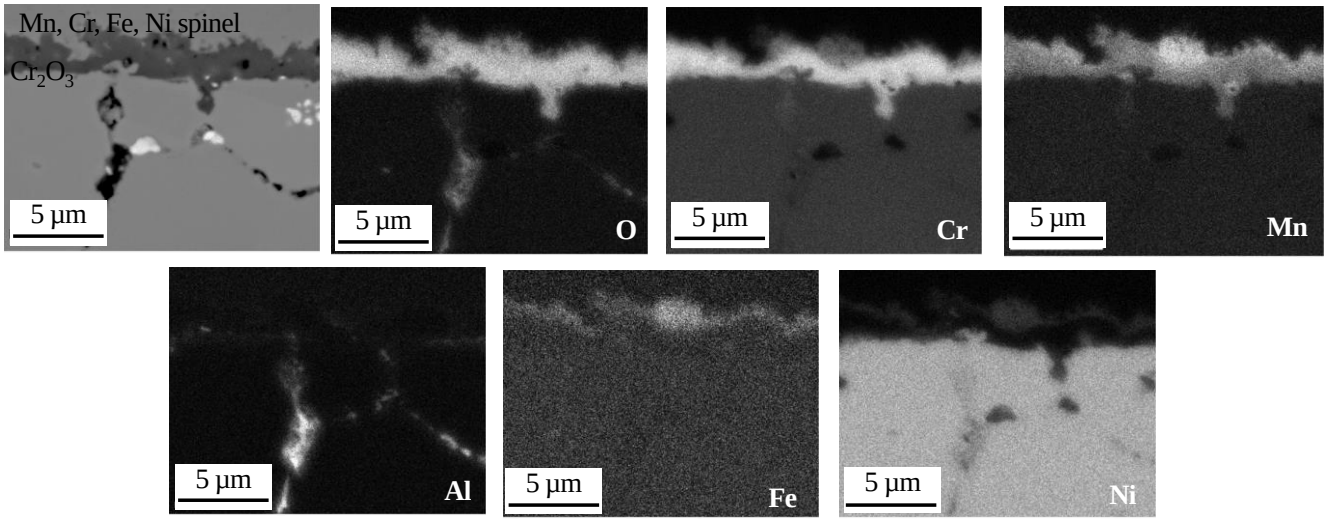

(c)

Figure 4: EDS elements maps of the oxide scale on the surface of (a) S31000, (b) N08120 and (c) N06230 specimens after 1,000 h of exposure in 100 h cycle air + 10 % H_2O at 850˚C.

No spinel was observed on the surface of the N06625 specimen, and its oxide scale was mainly Cr_2O_3. Nb enrichment, likely δ-Ni_3Nb [19], was observed underneath the oxide scale. In addition, internal oxidation of Al along the alloy grain boundaries was observed (Figure 3d and elemental maps in Figure 5).

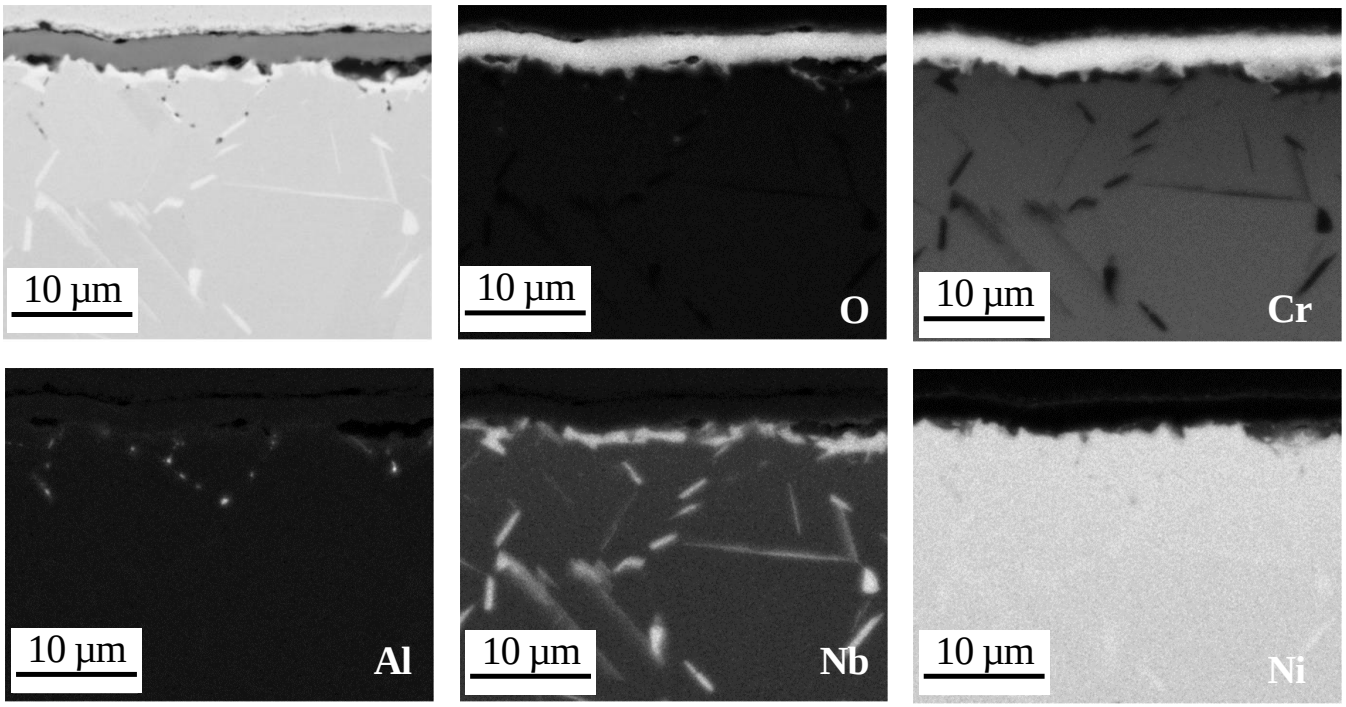

Figure 5: EDS elemental maps of the oxide layer on the surface of the N06625 specimen after 1,000 h of exposure in 100 h cycle air + 10 % H_2O at 850˚C.

An Al-rich oxide scale (likely Al_2O_3) formed on the surface of both AFA foils (BSE images in Figure 3e,f) but a Cr and Mn rich oxide spinel layer formed on top of the Al_2O_3 layer for the AFA 1 (Figure 6). These oxides were not present on the surface of the AFA2 specimen where only an Al-rich oxide scale, likely Al_2O_3, was observed (Figure 7).

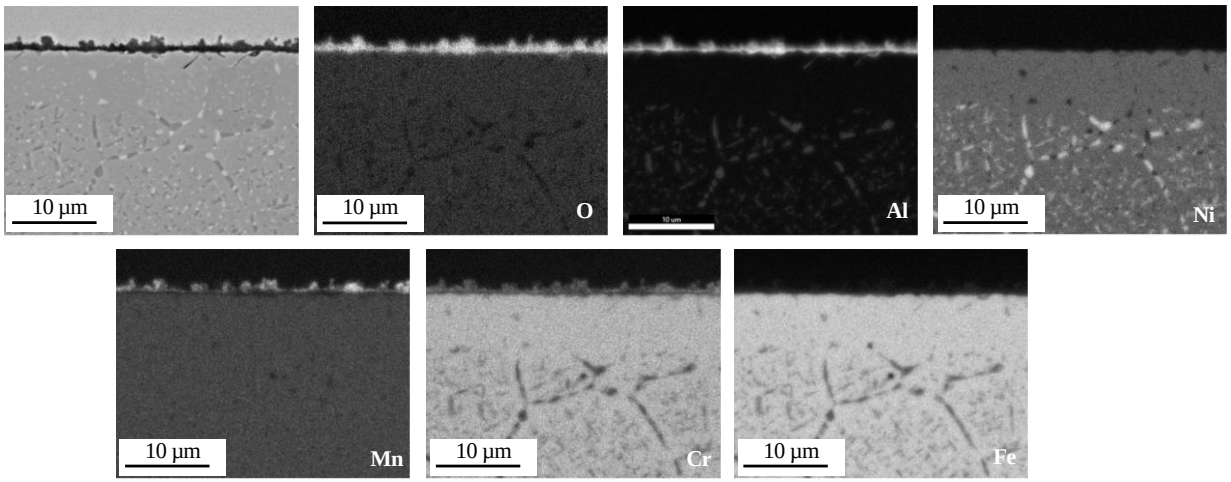

Figure 6: EDS elemental maps of the oxide scale on the surface of AFA1 specimen after 1,000 h of exposure in 100 h cycle air + 10 % H_2O at 850˚C.

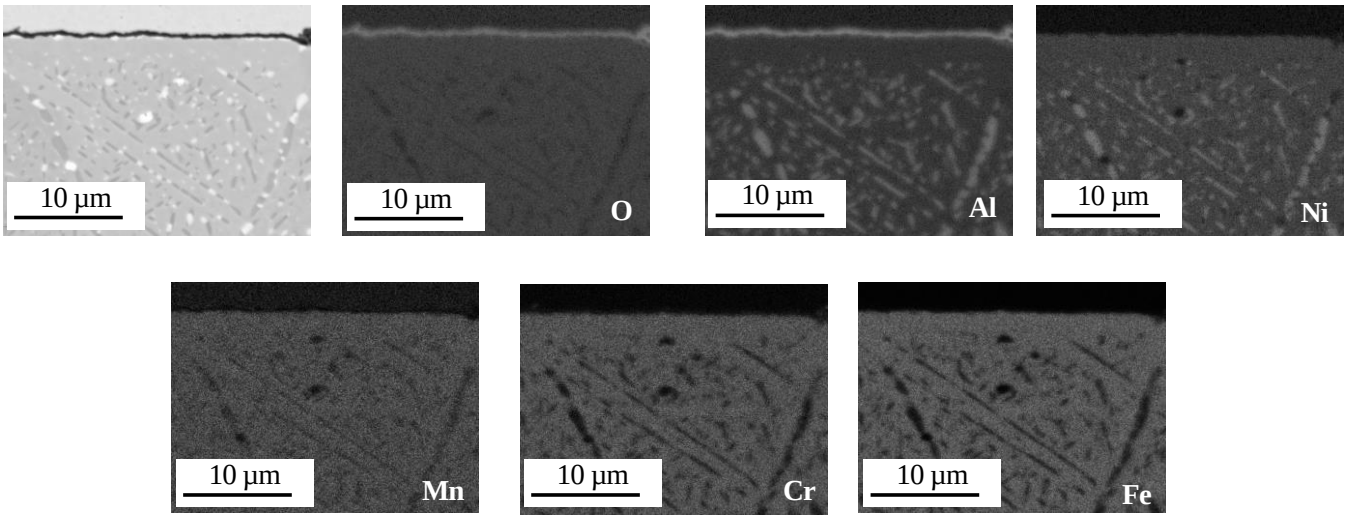

Figure 7: EDS elemental maps of the oxide scale on the surface of AFA2 specimen after 1,000 h of exposure in 100 h cycle flowing air + 10 % H_2O at 850˚C.

Underlying compositional changes

Under the oxide scales, Cr depletion profiles were measured and reported in Figure 8a after 1,000 h exposures at 850˚C. For the specimens where a Cr_2O_3 and Mn-rich spinel formed, Mn depletion profiles were also measured (Figure 8b). The depths of Cr and Mn depletion were the least for the N06230 foil (10 µm in Figure 8a,b). In addition, a Cr concentration of 18 wt.% (Figure 8a) and a Mn concentration of 0.4 wt.% (Figure 8b) were measured at the alloy-scale interface. A Cr concentration of 18 wt.% was also measured for the N08120 specimen but the Mn concentration was much lower, 0.1 wt. %. For the N06625 and S31000 specimens, Cr concentrations of about 15 wt.% were measured at the alloy-oxide interface (Figure 8a). Although 15 wt.% Cr was measured at the alloy-oxide interface of the alloy N06625, the specimen was not depleted in the center. S31000 and N08120 foils were also depleted in Cr in the center (18 wt.% and 22 wt.% 45 µm into the alloy in Figure 8a). These specimens were strongly depleted in Mn (Figure 8b). The Mn concentration in the center of the S31000 dropped sharply from 1.5 wt.% to 0.6 wt.% towards the alloy-oxide interface. For the N08120 specimen, a Mn profile was measured through almost half of the foil thickness, 45 µm in Figure 8b. For the AFAs, which formed an Al-rich oxide scale (Figure 6 and Figure 7), Al depletion profiles were measured in the underlying alloys. For the AFA1 alloy exposed for 3,000 h, an Al depletion profile was measured over 10 µm (Figure 9).

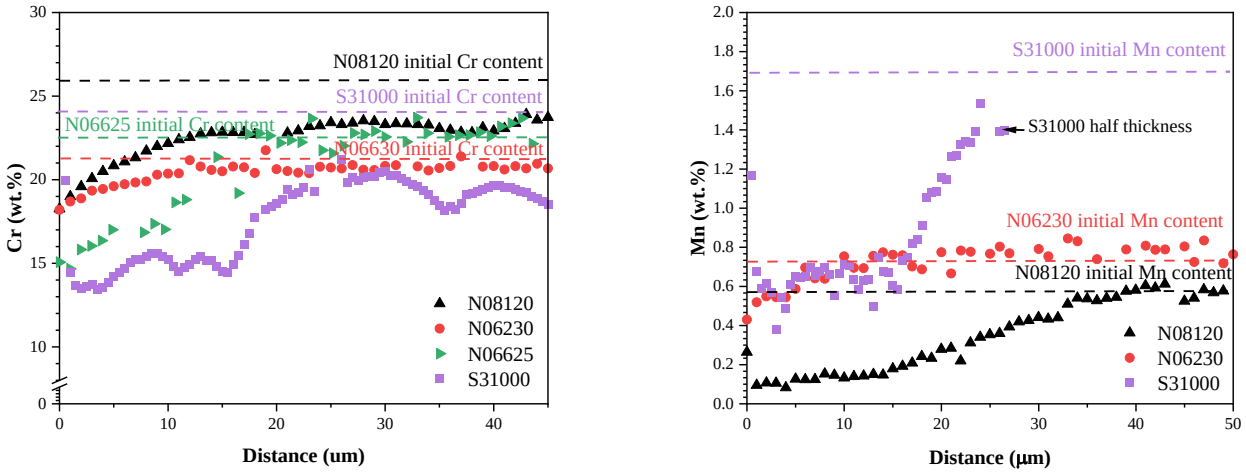

(a) (b)

Figure 8: (a) Cr and (b) Mn EDS profiles measured in the alloys N08120, N06230, N06625 and S31000 after 1,000 h of exposure in 100 h cycle flowing air + 10 % H_2O at 850˚C.

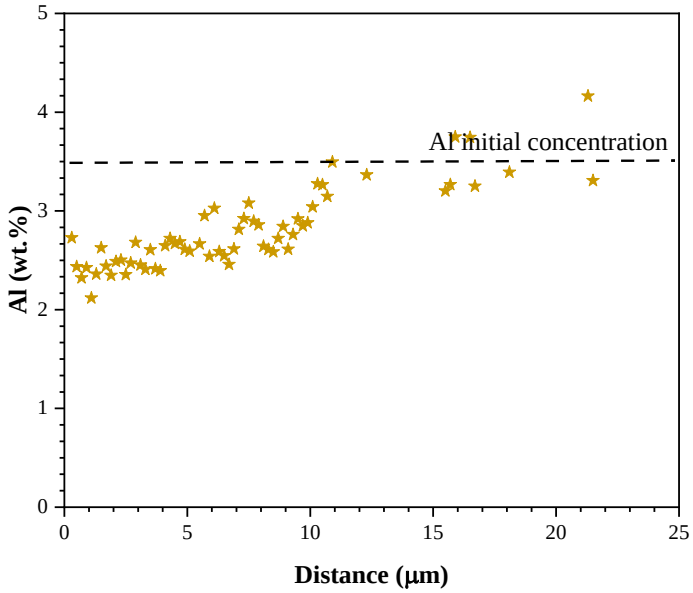

Figure 9: EDS Al elemental profile measured in AFA1 after 3,000 h of exposure in 100 h cycle flowing air + 10 % H_2O at 850˚C.

To compare the Cr consumption between alloys (later called Cr loss), the areas under the Cr depletion profiles for each specimen were integrated after various exposure times considering each alloy's density. The values were then normalized by the respective initial Cr reservoir, which corresponded to the foil thickness multiplied by its initial Cr content. For the Al_2O_3 formers (AFAs), the Al loss was also determined as a function of time and normalized to the initial Al reservoir in each foil. The results are reported in Figure 10a.Figure 9: EDS Al elemental profile measured in AFA1 after 3,000 h of exposure in 100 h cycle flowing air + 10 % H_2O at 850˚C.

The highest Cr loss was measured for the alloy S31000 reaching about 38 % Cr loss after 3,000 h in Figure 10a, which was consistent with the high mass gain observed for this material. The lowest Cr

loss (1 %) was observed for the N06230 foil after 3,000 h of exposure (Figure 10a). For the N08120 and N06625 specimens, Cr loss values of 25 and 20 % were measured respectively after 3,000 h. For the AFA specimens, about 4 % Al loss was measured after 3,000 h of exposure (Figure 10a).

The Cr or Al loss values were converted into sound metal loss which was defined as the metal loss by external oxidation (Cr_2O_3 or Al_2O_3) and Cr_2O_3 volatilization into $CrO_2(OH)_2$ in Figure 10b. Total metal loss of 6, 5.5 and 4 µm were obtained for the N08120, S31000 and N06625 specimens respectively after 3,000 h. The lowest metal loss values were calculated for the N06230 and AFA specimens, 0.4 and 0.2 µm respectively.

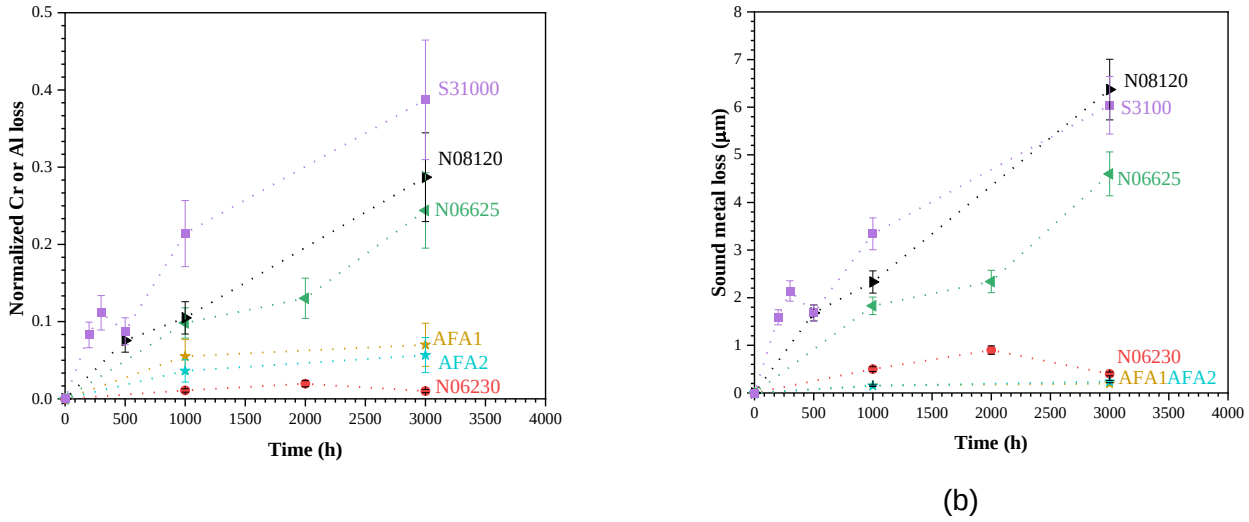

(a) (b)

Figure 10: Measured (a) Cr loss (S31000, N08120, N06230, N06625) or Al loss (AFA1, AFA2) normalized by their starting concentrations and (b) resulting sound metal loss as function of time in 100 h cycle flowing air + 10 % H_2O at 850˚C.

Even though the metal losses seemed low for all alloys, significant Cr loss was measured for S31000, N08120 and N06625 after 3,000 h. In addition, significant dissolution of strengthening precipitates in the foils was observed. As seen in Figure 11a, in the S31000 specimens, almost two thirds of the strengthening precipitates were dissolved after only 200 h of exposure at 850˚C and no precipitates were visible after the 3,000 h of exposure (Figure 11a). Slightly less precipitate dissolution was observed for the N08120 specimens where precipitates were still present after 3,000 h (Figure 11b). For these two alloys, voids were observed in the precipitate free zones (Figure 11a,b). A lower density of δ-Ni_3Nb precipitates was observed after 3,000 h than after 1,000 h of exposure in N06625 (Figure 11c). The thickness of the precipitate free zone in the N06230 and AFA specimens was lower than for the above mentioned foils and did not increase significantly with time (25 and 10 µm respectively after 3,000 h in Figure 11d,e). In addition, slight coarsening of the precipitates in the AFA1 specimen was observed between 1,000 and 3,000 h of exposure (Figure 11e). Using ImageJ software, the average area fraction of precipitates remained 17 ± 3 % while the precipitate size increase from 0.140 ± 0.20 μm^2 to 0.360 ± 0.20 μm^2 between 1000 and 3000 h of exposure.

S31000 – 200 h

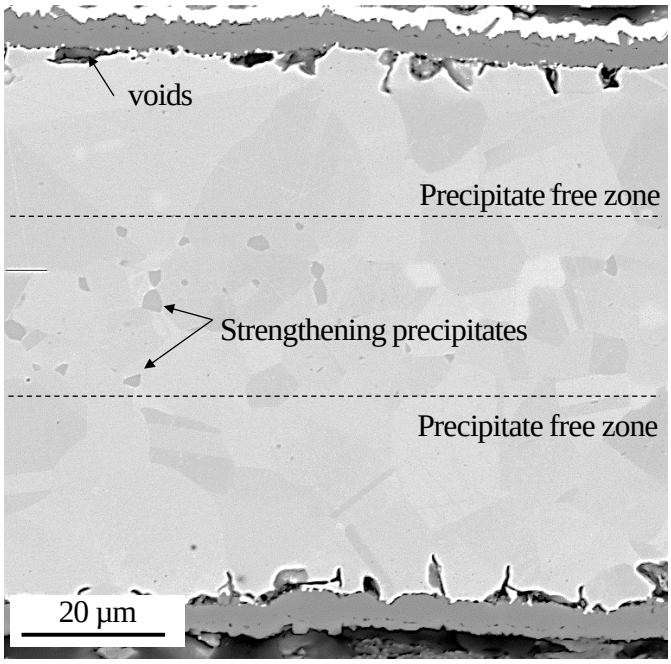

S31000 – 3,000 h

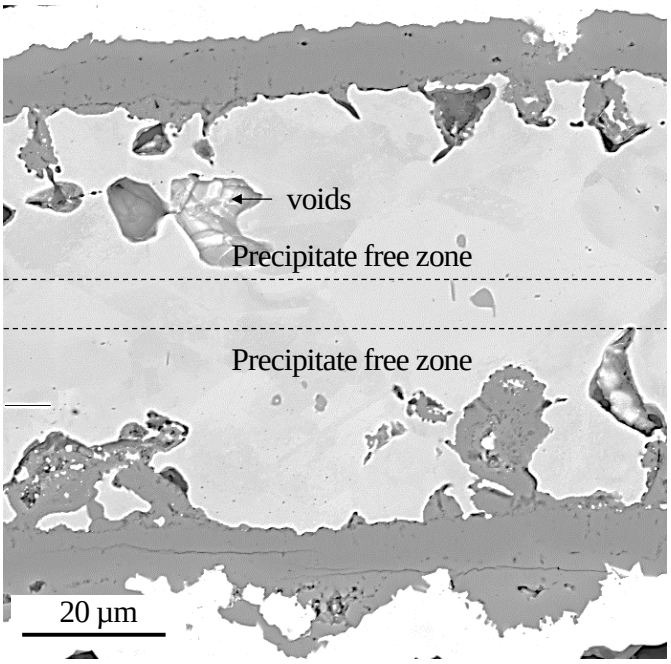

(a)

500 h – N08120

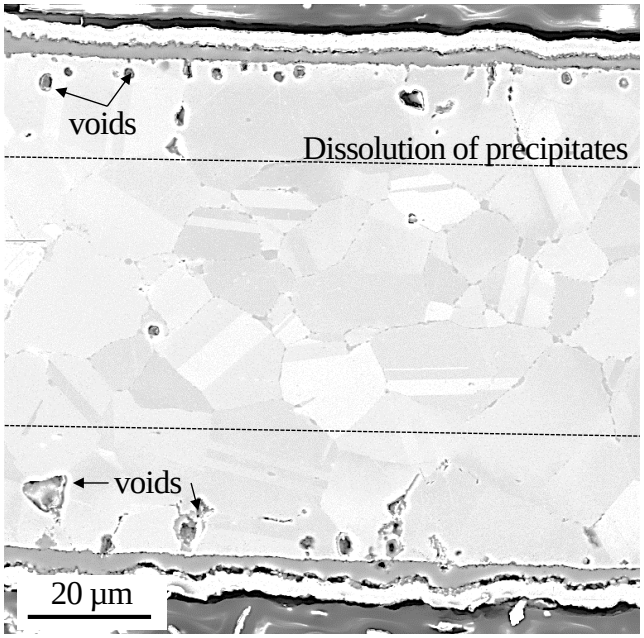

1,000 h – N08120

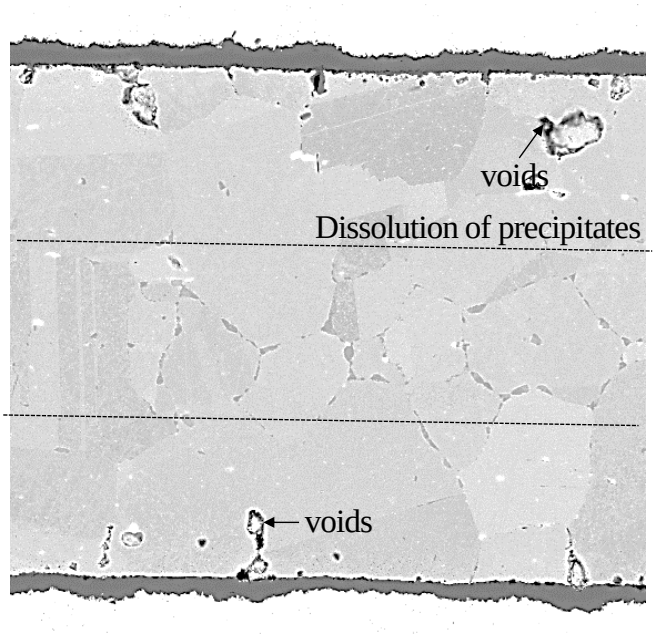

(b)

1,000 h – N06625

3,000 h – N06625

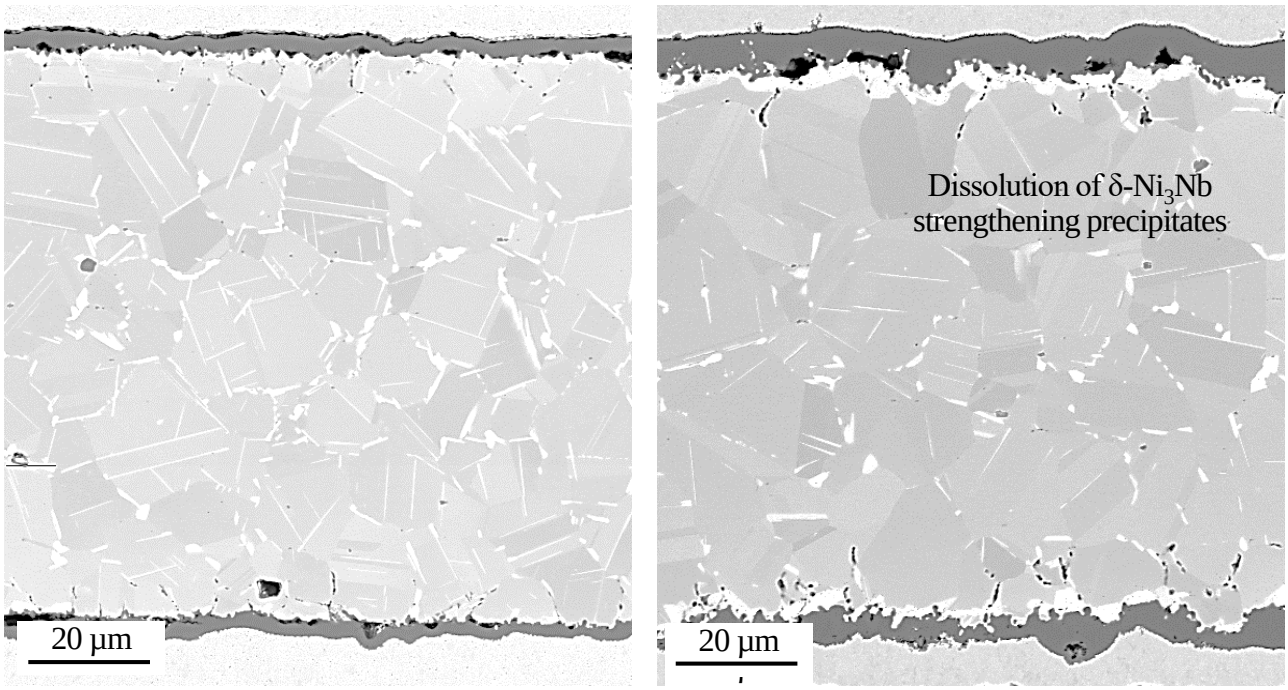

(c)

1,000 h – N06230

3,000 h – N06230

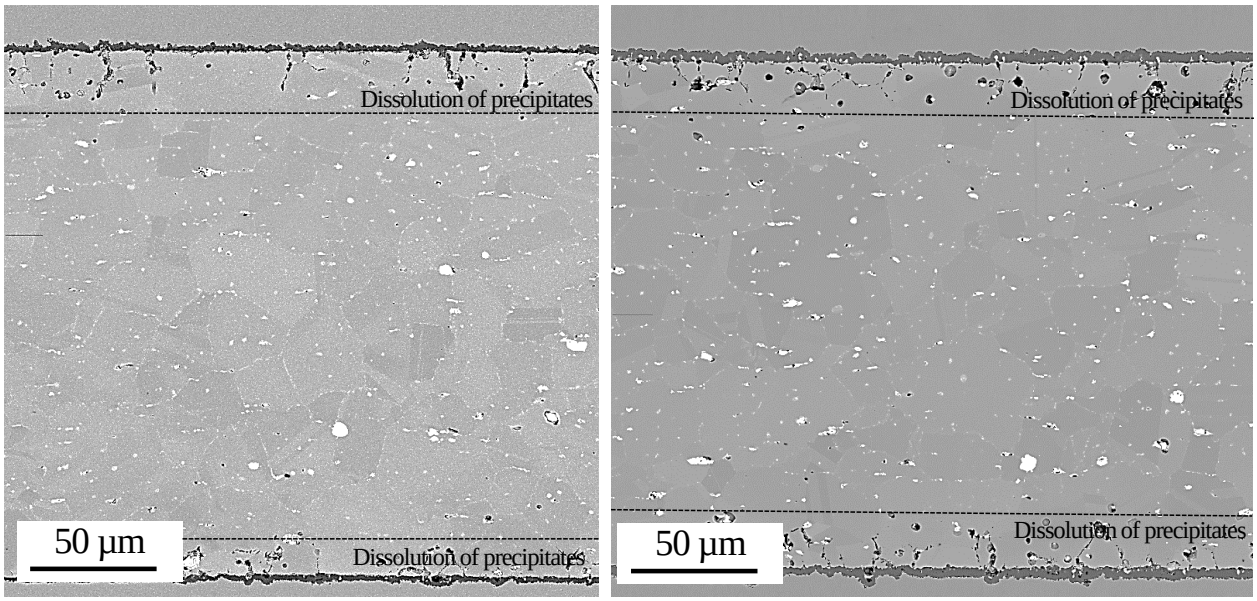

(d)

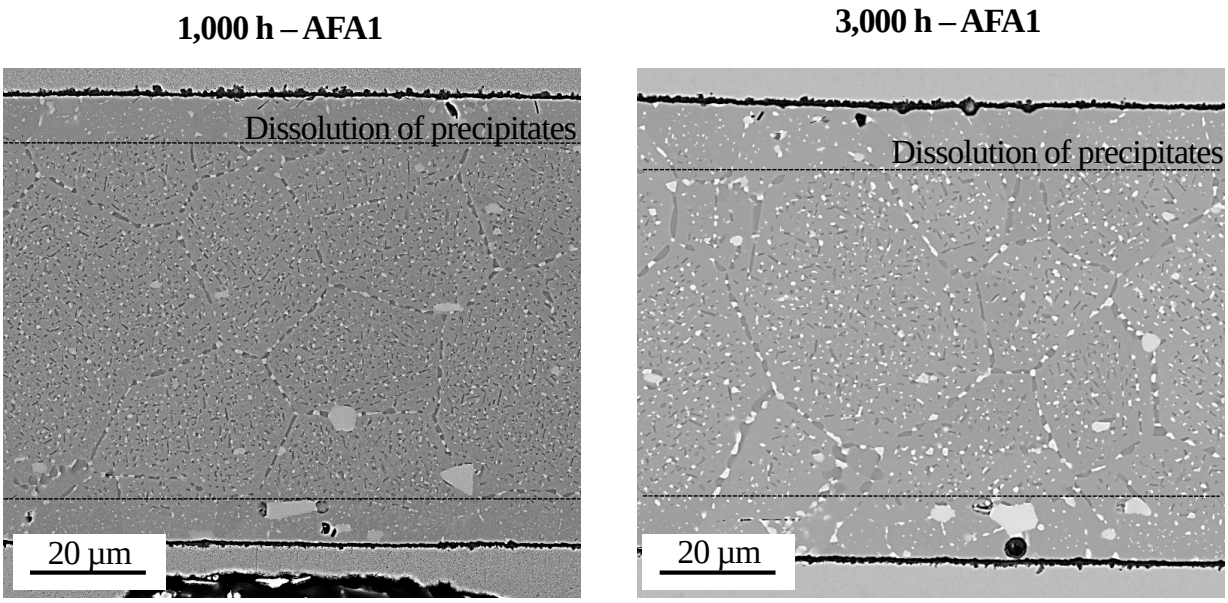

(e)

Figure 11: BSE images of (a) S31000, (b) N08120, (c) N06625, (d) N06230 and (e) AFA1 after various exposure times in 100 h cycle flowing air + 10 % H_2O at 850˚C.

Discussion

Effect of water vapor on protective oxidation behavior

Protective oxidation behavior is usually defined as the formation of slow growing oxide scales, typically Cr_2O_3 and Al_2O_3 [20]. In the presence of water vapor for the S31000 specimen, a transition from relatively low mass gain to high mass gain was observed at 850˚C associated with significant Cr (Figure 10) and Mn depletion in the foil (Figure 8b). As can be seen in Figure 12, the transition corresponded to the breakdown of the Cr_2O_3 oxide scale (Figure 12a), which started after about 2,500 h (Figure 12b), and the subsequent formation of thick Fe-rich external oxides and internal oxidation in some locations (Figure 12c). As also shown in Fig. 12, a similar transition was observed in dry and wet air at 800 ˚C and a breakaway occurred earlier in wet air than in dry air. These results indicated accelerated Cr depletion in wet air due to the combined effect of oxidation and volatilization of the Cr_2O_3 into $CrO_2(OH)_{2(g)}$ [8,9]. Accelerated Cr loss and earlier breakdown of the Cr_2O_3 scale was also observed for N08120 and N06625 after 10,000 h of exposure in flowing air + 10 % H_2O at 800˚C [21]. The observed para-linear oxidation behavior of the mass change of N06625 in Figure 2 and approximately linear Cr loss and sound metal loss evolution for the alloys S31000, N08120 and N06625 in Figure 8a indicated combined oxidation and volatilization of the oxide scale into $CrO_2(OH)_2$(g) [22]. However, at 850°C, the breakdown of the Cr_2O_3 scale formed on N08120 and N06625 was not yet observed after 3,000 h of exposure (BSE image and EDS maps in Figure 3d and Figure 5).

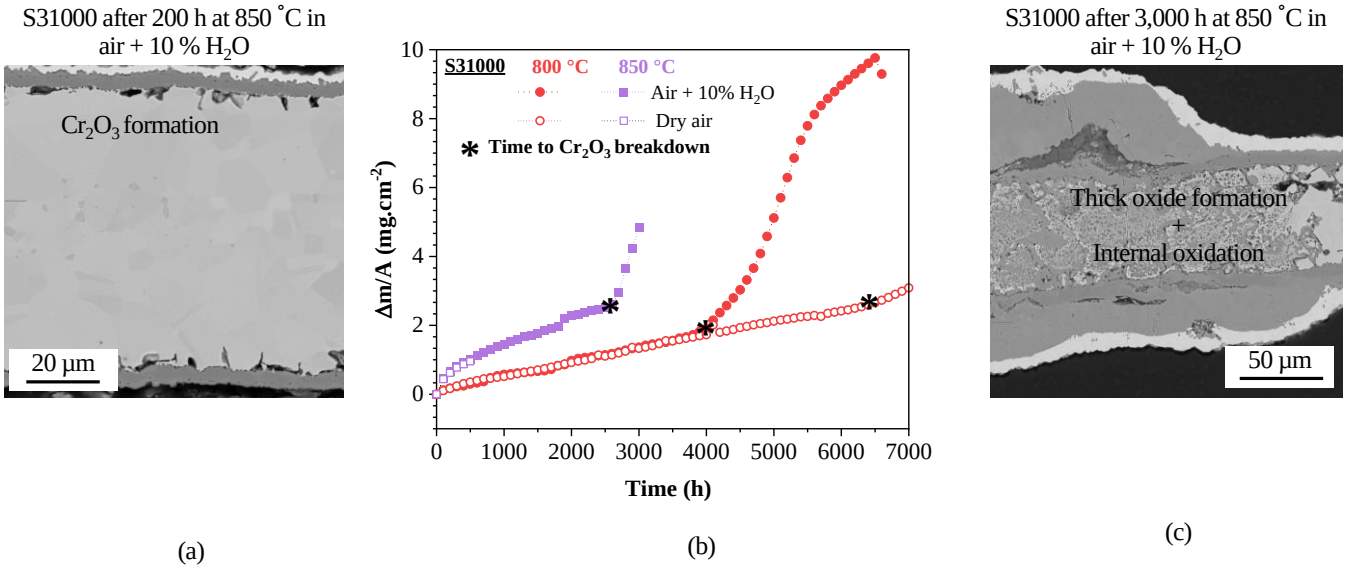

(a) (b) (c)

Figure 12: Effect of water vapor and temperature on Cr_2O_3 breakdown of S31000 foil exposed at 800 and 850 ˚C in 100 h cycle flowing air + 10 % H_2O.

Effect of the spinel formation on volatilization behavior

The N06230 foil which also formed a spinel oxide on top of the Cr_2O_3 scale (Figure 4) presented a lower mass gain than N08120 and S31000 in wet air (Figure 2), a parabolic evolution of the Cr and metal losses and the lowest Cr and metal loss among the Ni-based foils (Figure 10a, b). These observations suggested a lower oxidation rate and volatilization of the spinel and Cr_2O_3 oxide formed on the surface of the N06230 than for the alloys N08120 and S31000. In the current study, a (Cr,Mn)-rich spinel formed on S31000 foil but did not prevent the volatilization of the Cr_2O_3 scale and its breakdown into Fe-rich oxides. Similarly, a (Cr,Mn)-rich spinel formed on the surface of N08120 at 800 ˚C flowing air + 10 % H_2O but did not limit the Cr_2O_3 volatilization [20]. Conflicting results have been reported in the literature on the effect of the Mn-rich spinel on Cr_2O_3 volatilization. Deodeshmukh *et al.* [14] proposed that the Mn-rich spinel formed on top of the Cr_2O_3 scale inhibited the Cr_2O_3 volatilization of the N06230 foil exposed in flowing (500 $cm^3.min^{-1}$) air + 10 % H_2O (720 h cycle) at 871˚C. Thermodynamic calculations by Holcomb *et al.* [23] suggested that the formation of $MnCr_2O_4$ would reduce the volatilization of the oxide scale but no experimental verification of the theory was provided. In contrast, greater mass losses of porous and dense $MnCr_2O_4$ powders were measured by Stenzel *et al.* compared to Cr_2O_3 dense and porous powders after 1,000 h of exposure at 850, 950 and 1050 ˚C in flowing air + 10 % H_2O (347 $cm.h^{-1}$) [24]. In the current study, the fact that the spinel was enriched in Ni in the case of the N06230 specimen (Figure 4c) suggests a lower oxidation and volatilization rate for Ni, Mn and Cr-rich spinel (Figure 4c) than the Fe, Mn and Cr-rich spinel found on the surface of S31000 and N08120 specimens (Figure 4a,b) as discussed in [25]. The presence of La in N06230 also could help in slowing the oxidation rate of the Cr_2O_3 scale [26].

The Al_2O_3 scale formed on the surface of the AFA specimens was responsible for the observed lowest mass gain and metal loss (Figure 2 and Figure 10b). It is widely known that Al_2O_3 scales grow more slowly than Cr_2O_3 scales [20]. Furthermore, at 850˚C in 50% H_2O-50% O_2, the equilibrium partial pressure of the aluminum hydrate vapor species $Al(OH)_3$ is about three order of magnitude lower than the $CrO_2(OH)_2$ partial pressure [27]. These observations suggested that AFA foils could be well-suited as recuperator foils up to 850 ˚C.

Compositional and microstructural changes

Oxidation induced Cr or Al loss in air + 10 % H_2O led to the dissolution of the strengthening precipitates within each foil (BSE images in Figure 11). The formation of a precipitate dissolution zone

(PDZ) was reported in the literature for Ni based alloys [28-30]. In this study, the rate of precipitate dissolution was observed to be different between the Fe-based and Ni-based alloys. For carbides as precipitates, the depth of the carbide precipitation zone has been attributed to the oxidation-induced removal of Cr combined with the back diffusion of carbon from the alloy sub-surface to the specimen center [29, 30]. When precipitates were intermetallics, as observed in this study for alloy N06625 with δ-Ni_3Nb, the oxidation-induced loss of Cr was shown to induce the dissolution of the intermetallics in the center of the specimen and their diffusion and precipitation towards the alloy-oxide interface after exposure for 1000 h at 900 °C [19]. Although the total metal loss of the S31000, N08120 and N06625 foils did not exceed about 6 µm after 3,000 h of exposure at 850 ˚C in wet air, almost no strengthening precipitates remained in S31000, N08120 and N06625 alloys (BSE images in Figure 11a,b,c). In the N06230 and AFA specimens, a low fraction of the strengthening precipitates was dissolved below the formed oxide scale with slight coarsening of the precipitates in the AFA foils (Figure 11d,e). The slower growth and limited volatilization of the oxide scales formed on the N06230 (Cr_2O_3 and Ni, Mn, Cr spinel) and AFA (Al_2O_3) specimens than on S31000, N08120 and N06625 explain the lower extent of the precipitate dissolution zone in N06230 and AFA specimens.

CONCLUSIONS

The oxidation behavior of Fe-based and Ni-based foils in air + 10 % H_2O at 850˚C was investigated for up to 3,000 h exposures. Different oxidation induced Cr or Al loss kinetics were observed as a function of alloy composition and oxidation behavior. The austenitic stainless steel S31000, high Fe containing alloy N08120, and Ni-based alloy N06625 exhibited greater Cr loss than N06230 and AFA specimens. In addition, significant dissolution of strengthening precipitates was observed for S31000, N08120 and N06625 specimens but not for N06230 and AFA. The slow degradation rate of N06230 in the presence of water vapor was attributed to slow oxidation and volatilization kinetics of the Ni, Mn and Cr-rich spinel formed on the surface of the specimen in contrast to the Fe, Mn and Cr-rich spinel formed on the S31000 and N08120 alloys. The slow growth of the Al_2O_3 scale and its lower susceptibility to volatilization was responsible for low Al and metal loss of AFA specimens. These results suggest that N06230 and low cost AFA are promising candidates for creep and oxidation resistant microturbine recuperator operating up to 850˚C.

ACKNOWLEDGEMENTS

The authors would like to thank G. W. Garner, M. S. Stephens, T. Lowe, V. Cox at ORNL for their assistance with the experimental work and P. F. Tortorelli and M. Brady for their valuable comments on the manuscript. This research was sponsored by the U. S. Department of Energy, Office of Energy Efficiency and Renewable Energy, Combined Heat and Power Program. Notice: This manuscript has been authored by UT-Battelle, LLC under Contract No. DE-AC05-00OR22725 with the U.S. Department of Energy. The United States Government retains and the publisher, by accepting the article for publication, acknowledges that the United States Government retains a non-exclusive, paid-up, irrevocable, world-wide license to publish or reproduce the published form of this manuscript, or allow others to do so, for United States Government purposes. The Department of Energy will provide public access to these results of federally sponsored research in accordance with the DOE Public Access Plan (http://energy.gov/downloads/doe-public-access-plan).

REFERENCES

1. C.F., McDonald, “Recuperator considerations for future higher efficiency microturbines,” *Applied Thermal Engineering*, 23(12) (2003): p. 1463-1487.

2. B.A. Pint, K.L. More, R. M. Trejo, E. Lara-Curzio, “Comparison of recuperator alloy degradation in laboratory and engine testing,” *Journal of Engineering for Gas Turbines and Power-Transactions of the ASME*, 130(1) (2008).

3. T. Alberto, A. Massardo, “Optimal design of compact recuperators for microturbine application,” *Applied Thermal Engineering*, 25 (2005): p. 2054-2071.

4. P.J. Maziasz, J.P. Shingledecker, B.A. Pint, N. D. Evans, Y. Yamamoto, K.L. More, E. Lara-Curzio, “Overview of creep strength and oxidation of heat-resistant alloy sheets and foils for compact heat exchangers,” *Journal of Turbomachinery-Transactions of the ASME,* 128(4) (2006): p. 814-819.

5. P.J. Maziasz, B.A. Pint, J.P. Shingledecker, K.L. More, N. D. Evans, E. Lara-Curzio, “Improving high temperature performance of austenitic stainless steels for advanced microturbine recuperators,” Proceedings of ASME Turbo Expo 2004 Power for Land, Sea, and Air, GT2004-54239 (Vienna, Austria, 2004).

6. P.J. Maziasz, R.W. Swindeman, *“*Selecting and developing advanced alloys for creep-resistance for microturbine recuperator applications,” *Journal of Engineering for Gas Turbines and Power-Transactions of the ASME,* 125(1) (2003): p. 310-315.

7. M. D. Bender, R. C. Klug, “Comparison of Ni-based 625 alloy and ATI 20-25+Nb^{TM} stainless steel foils after long-term exposure to gas turbine engine exhaust,” Proceedings of ASME Turbo Expo 2014: Turbine Technical Conference and Exposition, GT2014-25334 (Dusseldorf, Germany 2014).

8. H. Asteman, J.-E. Svensson, M. Norell, L.-G. Johansson, “Indication of chromium oxide hydroxide evaporation during oxidation of 304L at 873 K in the presence of 10% water vapor,” *Oxidation of Metals*, 52(1-2) (1999): p. 95-111.

9. E.J. Opila, D.L. Myers, N. S. Jacobson, I. M.B. Nielsen, D.F. Johnson, J. K. Olminsky, M. D. Allendorf, “Theoretical and experimental investigation of the thermochemistry of CrO2(OH)(2)(g),” *Journal of Physical Chemistry A*, 111(10) (2007): p. 1971-1980.

10. R. Peraldi, B.A. Pint, “Effect of Cr and Ni contents on the oxidation behavior of ferritic and austenitic model alloys in air with water vapor,” *Oxidation of Metals*, 61(5-6) (2004): p. 463-483.

11. P. Huczkowski, W. Lehnert, H. H. Angermann, A. Chyrkin, R. Pillai, D. Grüner, E. Hejrani, W. J. Quadakkers, “Effect of gas flow rate on oxidation behaviour of alloy N06625 in wet air in the temperature range 900–1000 ˚C,” *Materials and Corrosion,* 68(2)(2017): p. 159–170.

12. B.A. Pint, K.L. More, R. Trejo, E. Lara-Curzio, “Comparison of Recuperator Alloy Degradation in Laboratory and Engine Testing” *Jounal of Engineering for Gas Turbines and Power,* 130(1) (2008)

13. D.J. Young, B.A. Pint, “Chromium volatilization rates from Cr_2O_3 scales into flowing gases containing water vapor”, *Oxidation of Metals,* 66(3-4) (2006): p. 137–153.

14. V. P. Deodeshmukh, “Long-Term Performance of High-Temperature Foil Alloys in Water Vapor Containing Environment. Part I: Oxidation Behavior,” *Oxidation of Metals*, 79(5) (2013): p. 567-578.

15. M.P. Brady, Y. Yamamoto, M.L. Santella, P.J. Maziasz, B.A. Pint, C.T. Liu, Z.P. Lu, H. Bei, " The development of alumina-forming austenitic stainless stells for high-temperature structural use," *The Journal of The Minerals, Metals & Materials Society (TMS),* 60 (2008)

16. Y.Yamamoto, M.Takeyama, Z.P.Lu, C.T.Liu, N.D.Evans, P.J.Maziasz, M.P.Brady, "Alloying effects on creep and oxidation resistance of austenitic stainless steel alloys employing intermetallic precipitates," Intermetallics, 16(3) (2008): p. 453 – 462.

17. B.A. Pint, S. Dryepondt, M.P. Brady, Y. Yamamoto, B. Ruan, R. D. McKeirnan, "Field and Laboratory Evaluations of Commercial and Next Generation Alumina-Forming Austenitic Foil for Advanced Recuperators", *Journal of Engineering for Gas Turbines and Power*, 138(12) (2016)

18. S. Dryepondt, B.A. Pint, "Validation of Lifetime Models for Recuparator Foils Through Long-Term Laboratory and Engine Testing," Proceedings of the ASME Turbo Expo 2019 Power for Land, Sea, and Air, GT2019-90927 (Phoenix, Arizona, USA, 2019).

19. A. Chyrkin, P. Huczkowski, V. Shemet, L. Singheiser, W.J. Quadakkers, "Sub-Scale Depletion and Enrichment Processes During High Temperature Oxidation of the Nickel Base Alloy N06625 in the Temperature Range 900–1000 °C," *Oxidation of Metals,* 75(2011): p. 143-166.

20. D.J. Young, *Chapter 1 - The Nature of High Temperature Oxidation*, in *High Temperature Oxidation and Corrosion of Metals,* Second Edition (Elsevier, 2016), 1-30.

21. M.M. Romedenne, R.R. Pillai, S. Dryepondt, B.A. Pint, "Effect of water vapor on lifetime of N06625 and N08120 foils during oxidation between 650 and 800 °C," **In Press**.

22. C. Tedmon, "The effect of oxide volatilization on the oxidation kinetics of Cr and Fe-Cr alloys," *Journal of the Electrochemical Society,* 113(8) (1966).

23. G. R. Holcomb, D.E. Alman, "The effect of manganese additions on the reactive evaporation of chromium in Ni-Cr alloys," *Scripta Materialia*, 54 (10) (2006): p. 1821-1825.

24. A. Stenzel, D. Fahsing, M. Schutze, M. c. Galetz, "Volatilization kinetics of chromium oxide, manganese oxide, and manganese chromium spinel at high temperatures in environments containing water vapor," *Materials and Corrosion-Werkstoffe Und Korrosion*, 70(8) (2019): p. 1426-1438.

25. R. Pillai, M. Romedenne, A. Haynes, B. Pint, "Oxidation behavior of candidate NiCr-alloys for engine exhaust valves - Part I: Effect of minor alloying elements", **In Press**

26. B. Pint, J. Keiser, "Alloy Selection for High Temperature Heat Exchangers," NACE CORROSION 2006, NACE-06469 (San Diego, California, USA, 2006).

27. E.J. Opila, "Volatility of Common Protective Oxides in High-Temperature Water Vapor: Current Understanding and Unanswered Questions," *Materials Science Forum*, 461-464 (2004): p. 765-774.

28. F. Gesmundo, B. Gleeson, "Oxidation of Multicomponent 2-Phase Alloys," *Oxidation of Metals*, 44(1-2) (1995): p. 211-237.

29. R. Pillai, H. Ackermann, H. Hattendorf, S. Richter, "Evolution of carbide and chromium depletion profiles during oxidation of Alloy 602 CA," *Corrosion Science*, 75 (2013): p. 28-37.

30. A. Chyrkin, R. Pillai, H. Ackermann, H. Hattendorf, S. Richter, W. Nowak, D. Grüner, W. J. Quadakkers, “Modeling carbide dissolution in alloy 602 CA during high temperature oxidation,” *Corrosion Science*, 96 (2015) 2015: p. 32-41.